Ripple propagation and velocity dispersion on ion-beam-eroded silicon surfaces

S. Habenicht* and K. P. Lieb
II. Physikalisches Institut and Sonderforschungsbereich 345, Georg-August-Universität Göttingen, Bunsenstr. 7-9, D-37073 Göttingen, Germany

J. Koch and A. D. Wieck
Lehrstuhl für Angewandte Festkörperphysik, Ruhr-Universität Bochum, Universitätsstr. 150, D-44780 Bochum, Germany
(Received 19 March 2001; revised manuscript received 4 September 2001; published 8 March 2002)

The propagation of surface ripples during Ga ion beam erosion of Si was measured in real time by combining focused ion beam technology with scanning electron microscopy. By detecting the secondary electrons emitted during implantation the surface was monitored *in situ* during the erosion. The ripple wavelength increases with the erosion time as $\lambda \propto t^{0.50(4)}$. The value of the ripple velocity was observed to agree qualitatively with the results of Monte-Carlo simulations of the erosion process, and was found to decrease with the ripple dimension like $v \propto \lambda_x^{-1.5(1)}$.

DOI: 10.1103/PhysRevB.65.115327 PACS number(s): 68.35.Bs, 61.80.Jh, 79.20.Rf

I. INTRODUCTION AND THEORETICAL ASPECTS

The surface morphology and its evolution during external treatments, e.g., ion beam erosion, is one of the dominating topics in surface physics. Ion beam erosion of solid surfaces arises as a consequence of the material removal during ion bombardment via sputtering of particles.[1] If the ion energy is sufficiently low, this sputtering phenomenon is the dominating mechanism governing the evolution of the surface morphology during ion beam treatment.[2] The sputtering yield depends on the local surface curvature in such a way, that for incident angles not to be near to grazing this dependency leads to a surface instability (sometimes called a negative surface tension) where the erosion velocity in depressions is greater than on mounds of the surface. On the contrary, competitive effects (with surface diffusion as the most prominent described by the surface mobility B) tend to smooth the surface topography, since they attempt to lower the surface roughness.[3] The interplay between these two effects is responsible for the creation of cones and dots on surfaces at normal ion incidence,[4] and especially for ripplelike and wavelike surface morphologies, when the direction of the ion beam is tilted to the surface normal.[5–8] In this context the projection of the ion beam onto the surface is named the x direction; the y direction is the perpendicular orientation. Several theoretical descriptions of surface erosion using ion beams have been developed, among them the most prominent ones by Bradley and Harper[9] and Cuerno and Barabasi[10,11] by means of stochastical differential equations. In all these descriptions the characteristic length on the surface, namely the ripple wavelength $\lambda_{x,y}$ [which means that waves occur in $x(\lambda_x)$ and y directions (named λ_y), depending on the angle of incidence of the ion beam] for oblique incidence, depends on both roughening and smoothing effects like $\lambda_{x,y} \propto \sqrt{B/|C_{x,y}|}$, where $|C_{x,y}|$ is the largest absolute value of the surface tension coefficients and B the smoothing coefficient (in most theories the surface mobility[12]). Following the theoretical concepts of Bradley, Harper, Cuerno, and Barabasi,[2,9,10] the surface height evolution $h(\mathbf{r},\mathbf{t})$ can be described as

$$\frac{\partial h}{\partial t} = -F_0 + C\frac{\partial h}{\partial x} + C_x\frac{\partial^2 h}{\partial x^2} + C_y\frac{\partial^2 h}{\partial y^2} + \Lambda_x\left(\frac{\partial h}{\partial x}\right)^2 + \Lambda_y\left(\frac{\partial h}{\partial x}\right)^2 - B\nabla^4 h + \eta. \quad (1)$$

F_0 defines the surface erosion rate of a flat surface at normal incidence ($F_0 = \Phi Y_0/n$), which is directly related to the sputtering yield Y_0 of a flat surface. $C\partial h/\partial x$ is a term related to the derivative of the sputtering yield with respect to the angle of incidence, $C_{x,y}\partial^2 h/\partial x,y^2$ describes the linear curvature dependence of the surface erosion, with $C_{x,y} = (\Phi a Y_0/n)\Gamma_{x,y}$, $\Lambda_{x,y}(\partial h/\partial x,y)^2$ being the nonlinear contribution; $B\nabla^4 h$ is the surface diffusion according to Wolf-Villain and Mullins.[3] η defines the noise terms corresponding to the implantation process. Several aspects of this theory have been examined experimentally on various surfaces using scanning probe microscopy (scanning tunneling microscopy, AFM) (Refs. 13–16, 20, 32) and light spectroscopy.[17–19] Although many topics like the microscopic nature of surface smoothing are still under discussion the physical background of ion beam erosion is well understood compared to similar erosion phenomena in nature.

However, among other features still unknown in this context, one severe aspect of the theory has been failed to observe up to now: As a consequence of the broken symmetry when tilting the ion beam to the surface normal, the ripple fronts should propagate in the direction of the ion beam projection,[9,11] a phenomenon which is clearly known in the nature of wind blowing over granular surfaces. To see if this propagation can also be observed on surfaces patterned by erosion on a nanometer scale would be a fascinating topic in surface studies. In fact, this propagation has been predicted by Monte-Carlo simulations of the erosion process in former publications.[12,21] One obtains surface ripples with wavelength λ_x moving into the direction of the ion beam with a propagation velocity v like

$$h(t) = -F_0 t + A(t)\exp\left[i\left(\frac{2\pi}{\lambda_x}x - \omega t\right)\right], \quad (2)$$

$$\omega = \frac{2\pi v}{\lambda_x}.$$

F_0 and $A(t)$ are physical constants related to the ion flux and the initial surface morphology.[9] The erosion theory exhibits a linear velocity dispersion for the ripples, which means that the propagation velocity v of the ripples should be independent of the ripple wavelength λ_x. This propagation at constant velocity, if it could be observed, should be a clear indicator that the evolution of the surface morphology is governed by linear terms of surface erosion; deviations would indicate the importance of nonlinear contributions to the theory.[2] In order to observe this propagation, one has to monitor the evolution of the surface morphology resolved in time over a sufficiently long period without any drift or location problems for sample and scanner: requirements which cannot be achieved by probe microscopy or spectroscopy techniques.

II. EXPERIMENTAL DETAILS

For this reason, in the following experiments the evolution of (100)-silicon surfaces was monitored *in real time* using the secondary electron emission from the surface induced by either a focused electron beam (namely scanning electron microscopy SEM) or a focused ion beam (named focused ion beam microscopy, FIBM).[22] In the latter case, as the innovative topic, the same ion beam, a 30 keV Ga^+ beam with a minimum spot diameter of about 30 nm, was used simultaneously for surface erosion and surface microscopy. The technique to use the secondary electron emission from focused ion beams for surface micropscopy is described elsewhere in detail.[23,24] A square of 10×10 μm^2 was exposed to the ion beam under a tilt angle of 30° relative to the surface normal. In order to provide the evolution of correlations of the surface topography orders of magnitude above the size of the beam spot, the whole exposed area was scanned by the ion beam with a 25–100 Hz-repetition rate (which means that each point of the implanted area is met up to a hundred times in a second with a dwell time on each point of several microseconds). Therefore, within a time scale of seconds, which is important for erosion experiments, the ion beam current can be estimated to be constant in time and homogeneous over the exposed area accounting for a coherent implantation of the whole square within even small sections of the erosion time. The typical ion current density was 7.5×10^{14} $cm^{-2}s^{-1}$ (the current density has been varied between 10^{14} and 10^{15} $cm^{-2}s^{-1}$) over the whole exposed area, which corresponds to a spot current of ca. 15 A/cm^2 for the focus of the beam. The influence of such an ion irradiation on the surface temperature can be estimated using the calculation of Melngailis.[25] If a thermal conductivity of 1.5 W/cmK is assumed for Si, the temperature increase of the distinct irradiated surface area is about 2 K for the beam exposing a single spot and far below 1 K for the beam scanned over the region mentioned above. If the average over the whole exposed area is taken, the influence of the ion irradiation on the surface temperature is negligible. In contrast, the secondary electrons are detected for every distinct scanning point of the ion beam and this effect can be added to a picture of the whole surface area.

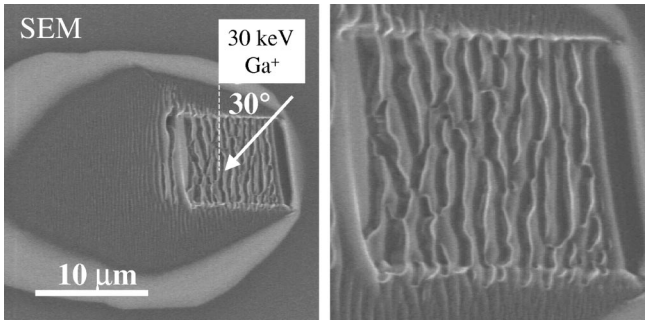

FIG. 1. Scanning electron microscopy pictures of the silicon surface after erosion with a 30 keV Ga^+ focused ion beam with a spot size of 30 nm. The angle of incidence was 30° relative to the surface normal; the total implantation fluence was 5×10^{18} ions/cm^2. The dimensions of the implanted square are 10×10 μm^2. The ripple morphology is clearly visible. Also the implantation halo induced by tails of the beam spot and eroded material can be seen.

III. RESULTS AND DISCUSSION

Figure 1 shows a typical SEM picture of the exposed region on the surface. The implantation fluence was 5×10^{18} ions/cm^2. The implanted and eroded square area of 10×10 μm^2 is clearly visible, surrounded by an implantation halo caused by the spot tails of the focused ion beam and eroded material from the exposed area.[26] Also the ripple morphology caused by the oblique incidence is visible, showing the interplay between surface roughening and surface smoothing. This ripple morphology is visible within the implanted square area as well as in the halo area caused by the spot tails of the focused ion beam. Whereas the ripple spacing within the square is homogenous over the exposed area, in the spot tails a continuous decrease of the ripple spacing can be observed (please see Fig. 2 for a comparison of the spacing inside and outside of the exposed area). This can be explained by the ion beam fluence, which decreases continuously with raising the distance from the border of the exposed area.[26,27] This behavior is in agreement with theoretical models of ion beam erosion and goes in parallel with former experiments regarding the fluence behavior of ion-beam-eroded surfaces (in the following this topic will be examined in further detail). Although it is not clear which smoothing mechanism is the dominant effect in these experiments—different scenarios like radiation enhanced diffusion and heating are possible among others[28,12]—the occurrence of the ripple morphology shows clearly that surface erosion as described above is present in this case. These SEM pictures can also be taken for comparison with the FIBM micrographs, shown in the following, especially to verify that thermal drift of the sample relative to the ion beam can be excluded for the interpretation. At this point it should be worth stating that without rapidly scanning the focused ion beam over the surface no long-range order correlation on the surface can be established and no ripple mor-

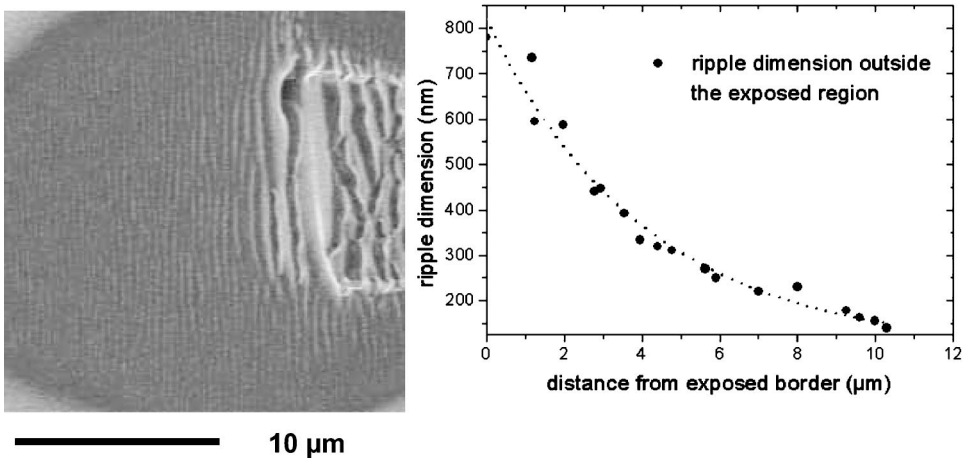

FIG. 2. Scanning electron picture (right) of the spot tail behind the exposed square. The decrease of the ripple wavelength can be clearly seen. (Left) Ripple wavelength as a function of the distance from the exposed area.

phology can be generated. In this case, if every point of the implanted area would be exposed with the whole ion dose at one time and the ion beam would scan one point after another in this manner, the scenario would completely differ from a homogeneous and coherent implantation which is necessary for the formation of long-range order in surface morphology. Especially the sputtering yield as well as the ion flux at a certain surface point would be a function of time. Therefore, continuum equations as mentioned above would hardly be applicable to describe such a scenario of surface erosion. If the focused ion beam is rapidly scanned over the exposed region, the irradiation is comparable to a normal homogeneous implantation of the whole region. In this case, a continuous irradiation of the area with a nonfocused ion beam can be seen as the ergodic limit of the short-time periodic exposure of each point of the implantation area. This limit has been reached, if the scanning velocity of the focused ion beam exceeds the diffusion velocity of adatoms on the exposed surface by orders of magnitude. This condition is valid in this case, therefore, all theories of ion beam erosion and its surface morpholgy evolution can be applied to the experimental scenario used in this work. Within the variation of the beam current density mentioned above, no change of the physical scenario has been observed. In Fig. 3 a typical FIBM micrograph is shown, where also the ripple morphology is visible. The sections observed with FIBM are sufficiently smaller than the exposed area to avoid boundary effects to superimpose the results. In this case the ion fluence was 1×10^{18} ions/cm^2 (which corresponds to an exposition time of 1400 s). The calculated autocorrelation function and its Fourier transform $S(k)$ prove the periodic character of the surface topography and can be used for a precise determination of size and orientation of the wave vector $k=k_x$ and therefore of the ripple spacing λ_x. The line shape of a cut through the Fourier transform along the spots (shown in the graph of Fig. 3) fits to the assumptions of the erosion theory by Bradley and Harper (see Refs. 9 and 29). Figure 4 shows pictures of the eroded surface taken by FIBM with rising erosion time. Two distinct effects can be observed. On the one hand, the major ripple wavelength increases with rising erosion time from 60 to 800 nm. This effect has been proposed theoretically[30,31] and previously observed experimentally.[32] The correlation length of the surface morphology (which in fact is the ripple wavelength in this case) is increased with the erosion time. The FIBM observation technique allows for the first time, to the best of our knowledge, to monitor this evolution over several orders of magnitude in real time. The scaling law of this development, which is an indicator for the strength of nonlinear contributions, is shown in Fig. 5(a). Assuming a power law $\lambda_x \propto t^b$, one obtains $b=0.50(4)$, which is in qualitative agreement with theoretical results of nonlinear growth during surface erosion.[30,31,33] The other effect is the propagation of the ripple fronts in the direction of the ion beam projection onto the surface, which is clearly visible in the serial pictures of Fig. 4. The ripples shown in the pictures move into the di-

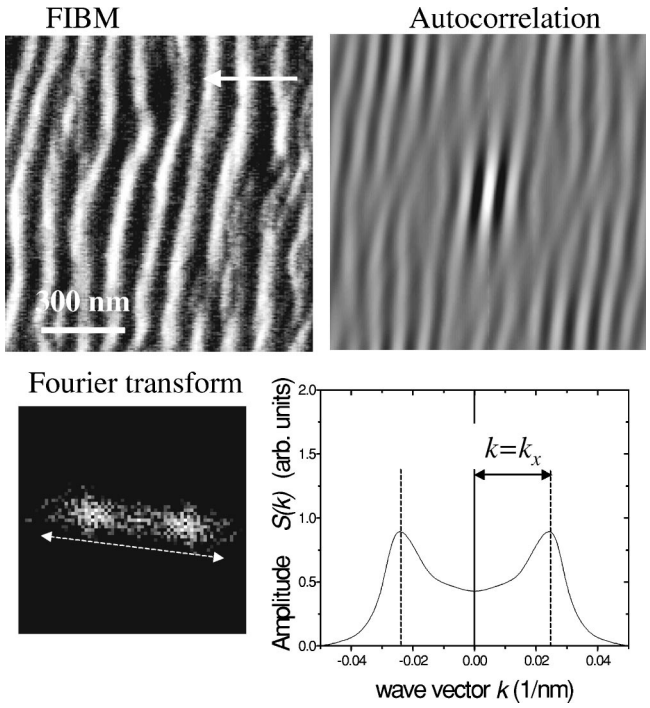

FIG. 3. Focused ion beam micrograph of the exposed region at an erosion time of $t=1400$ s, which corresponds to an ion fluence of 1×10^{18} ions/cm^2. The autocorrelation and its Fourier transform are added to prove the periodic surface structure. The graph shows a cut through the spots of the Fourier transform. The line shape fits to the assumptions of the theory of Bradley and Harper.

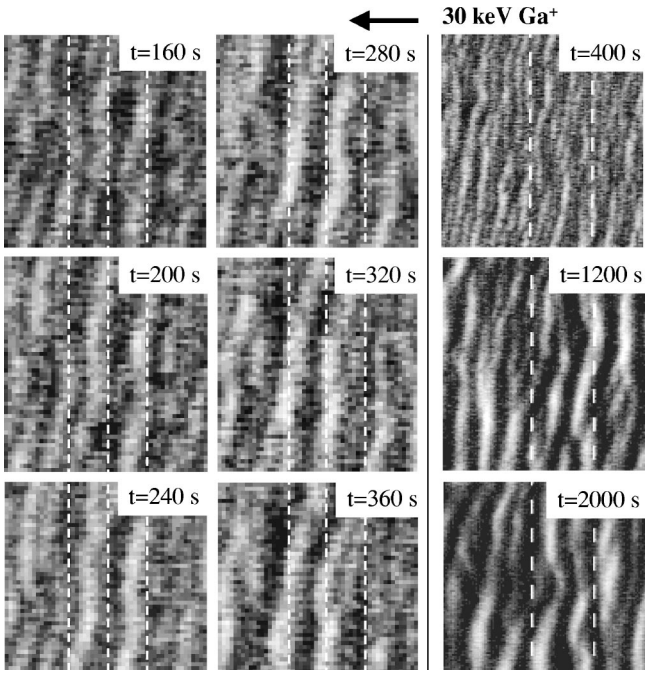

FIG. 4. Focused ion beam micrographs of the exposed silicon surface while exposed to a 30 keV Ga^+ ion beam. The projection of the ion beam onto the surface is given in the pictures. Following the pictures with rising erosion time (left and middle column) the ripple propagation from the right to the left is visible (the dashed lines are drawn to guide the eyes). With successively rising erosion time also the rising of the ripple wavelengths can be seen (right column). See the EPAPS movies (Ref. 34) 1 and 2.

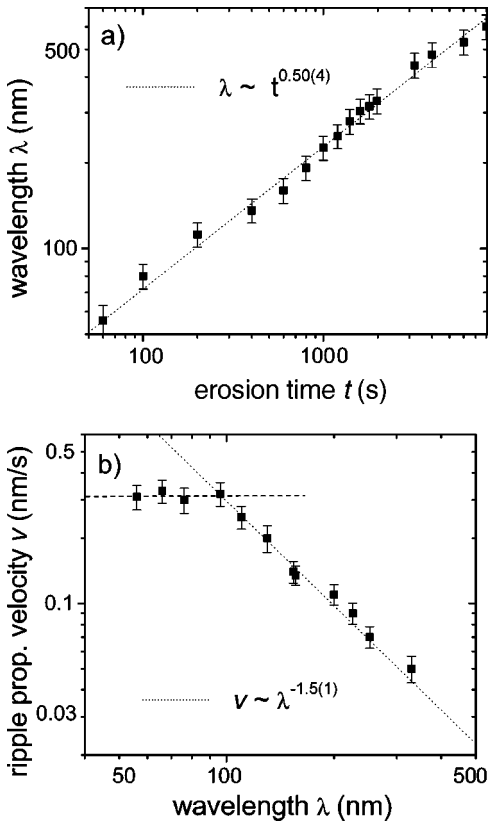

FIG. 5. Upper graph: Measured ripple wavelength λ in the FIBM pictures as a function of the erosion time *t*. The scaling law approximated to the data points to a nonlinear behavior in the evolution of the surface morphology. Lower graph: Measured velocity dispersion of the ripple propagation with rising wavelength. This decrease is a clear indicator for rising nonlinear contributions with rising erosion times.

rection of the ion beam, the velocity can be determined to be $v=0.33(4)$ nm/s for the small wavelengths and the experimental conditions chosen in this case. This propagation is proposed by the linear evolution theory and expresses the qualitative agreement with the descriptions by Bradley and Harper and Cuerno and Barabasi. In fact, this propagation and its mode velocity ω is of the same size as proposed in the Monte-Carlo results of ion-beam-eroded carbon surfaces by Koponen *et al.*,[12] which points also to a good agreement between computer simulations and experiments. However, as the ripple wavelength increases with rising erosion time, one observes a nonlinear velocity dispersion of the propagation, which means a continuous decrease of the ripple velocity [see Fig. 5(b)]. For the largest wavelengths $\lambda_x \geqslant 400$ nm, no further propagation is visible within the observed time scale. In fact, as also smaller ripples occur sporadically between the major wavelengths, they start to catch up with the major fronts and vanish into the flanks. A scaling law approximated to the data exhibits an observed velocity dispersion of $v \propto \lambda_x^{-1.5(1)}$ above a certain ripple wavelength, which means a certain erosion time in this case. Up to this wavelength and erosion time the velocity is nearly constant; only above this value a decrease is visible. This decrease cannot be explained by theory up to now. In fact, it might be an indication for a continuous transition to a rising nonlinear contribution in surface erosion. Since these dominant nonlinear terms depend on the square of the local surface slopes, these supplementations are known to scale down the breaking of symmetry in the beam direction. Therefore, between the linear and the nonlinear regime there has to be a continuous crossover which is expressed by the observed velocity evolution. Theoretical approaches indicate that a decrease of the ripple velocity with rising wavelength should take place[11] and therefore identify the observed effect of the velocity dispersion to be of a nonlinear origin.

Another interesting behavior can be observed if an already produced ripple morphology is subsequently irradiated with the 30° tilted ion beam which is rotated by 90° in azimuthal orientation. At the beginning of this irradiation the ripple orientation goes in parallel with the ion beam projection onto the surface. With rising erosion time one can observe first the vanishing of the ripple orientation and afterwards the development of the new ripple morphology with the new orientation perpendicular to the ion beam projection. This changing of the ripple orientation by changing the ion beam direction shows the influence of the noise which is present in the morphology evolution and induced by the ion beam. The new morphology is generated out of this noise and grows with rising fluence. Therefore the old ripple orientation can be destroyed and substituted by a new one with perpendicular orientation. Figure 6 shows FIBM pictures from surfaces during such an irradiation procedure. At first

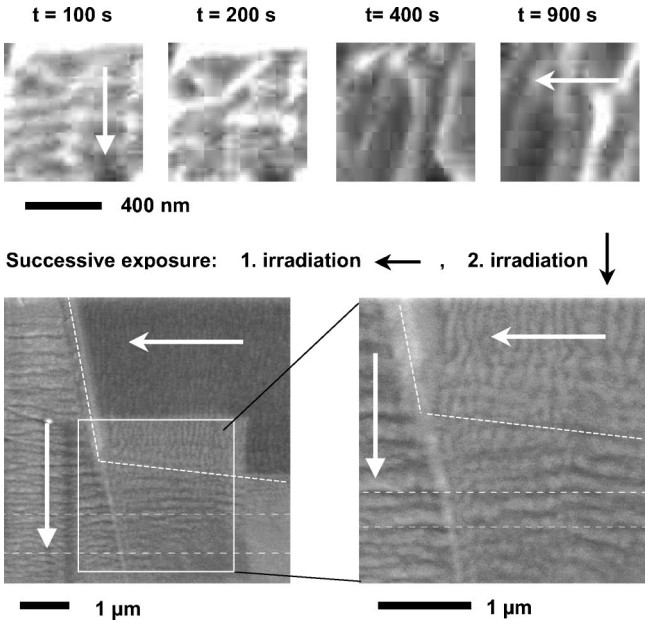

FIG. 6. Upper graph: FIBM pictures of a rippled surface during erosion by a rotated ion beam. Within the pictures the changing of the ripple orientation according to the new ion beam orientation can be seen. Lower graph: SEM pictures of the surface after successive irradiations. At the borders of the exposed area the change in orientation can be seen. See the EPAPS (Ref. 34) movie 3.

the old ripple orientation parallel to the ion beam projection can be seen, then the ripples vanish with successive irradiation, while after a certain time and ion fluence the orientation has changed to a perpendicular arrangement relative to the ion beam. This can also be seen looking at SEM pictures (see Fig. 6) of the borders of such a successively exposed region after the irradiation has been finished. In the irradiated area the new orientation is visible while outside the old ripples with perpendicular orientation can be seen. In the vicinity of the interface, also a transition regime is visible which originates from the spot tails of the focused ion beam. These pictures give a decisive insight into the dynamics of this noise driven transition between the distinct surface morphology orientations. In particular, they show the ability of a description of the mechanism of surface erosion by stochastical differential equations.

IV. CONCLUSIONS

In summary, the present observations of the ripple propagation and its velocity dispersion with rising wavelengths give new experimental insights into the microscopic and real-time behavior of nonequilibrium surface topographies. Using focused ion beam microscopy for initiating and documenting sputter erosion with high time and space resolution has led to the observation of new and distinct nonlinear effects. In fact, these results show interesting parallels between different effects of structuring and pattern formation in nature. Furthermore, the combination of focused ion beam treatment and microscopy of solid surfaces will enable further interesting experiments in the near future: By changing the implantation conditions, especially the spot size of the ion beam and the sweeping frequency over the exposed region, one will be able to observe the onset of the formation of surface correlations, such as ripple and dot formations, and will gain new information on the long- and short-range order in the surface morphology evolution.

This work was funded by the Deutsche Forschungsgemeinschaft.

*Present address: Philips Semiconductors Germany, Stresemannallee 101, D-22529 Hamburg, Germany, email: soenke.habenicht@philips.com

[1] P. Sigmund, in *Sputtering by Particle Bombardment I*, edited by R. Behrisch and K. Wittmaack (Springer Verlag, Heidelberg, 1981).
[2] A. L. Barabasi and H. E. Stanley, *Fractal Concepts of Surface Growth* (Cambridge University Press, Cambridge, 1995).
[3] D. E. Wolf and J. Villain, Europhys. Lett. **13**, 389 (1990); W. W. Mullins, J. Appl. Phys. **28**, 333 (1957).
[4] S. Facsko, T. Dekorsky, C. Koerdt, C. Trappe, H. Kurz, A. Vogt, and H. L. Hartnagel, Science **285**, 1551 (1999).
[5] G. Carter, M. J. Nobes, F. Paton, J. S. Williams, and J. L. Whitton, Radiat. Eff. **33**, 65 (1977).
[6] G. Carter, V. Vishniyakov, and M. J. Nobes, Nucl. Instrum. Methods Phys. Res. B **115**, 440 (1996).
[7] G. Carter and V. Vishnyakov, Phys. Rev. B **54**, 17 647 (1996).
[8] E. Chason, T. M. Mayer, B. K. Kellerman, D. T. McIlroy, and A. J. Howard, Phys. Rev. Lett. **72**, 3040 (1994).
[9] R. M. Bradley and J. M. E. Harper, J. Vac. Sci. Technol. A **6**, 2390 (1988).
[10] R. Cuerno and A. L. Barabasi, Phys. Rev. Lett. **74**, 4746 (1995).
[11] M. Makeev, R. Cuerno, and A. L. Barabasi (unpublished).
[12] I. Koponen, M. Hautala, and O. P. Sievänen, Phys. Rev. Lett. **78**, 2612 (1997).
[13] S. Habenicht, W. Bolse, K. P. Lieb, K. Reimann, and U. Geyer, Phys. Rev. B **60**, R2200 (1999).
[14] S. Habenicht, K. P. Lieb, W. Bolse, U. Geyer, F. Roccaforte, and C. Ronning, Nucl. Instrum. Methods Phys. Res. B **161-163**, 962 (2000).
[15] S. Habenicht, W. Bolse, H. Feldermann, U. Geyer, H. Hofsäß, K. P. Lieb, and F. Roccaforte, Europhys. Lett. **50**, 209 (2000).
[16] S. Rusponi, G. Costantini, C. Boragno, and U. Valbusa, Phys. Rev. Lett. **81**, 2735 (1998).
[17] R. Schlatmann, J. D. Shindler, and J. Verhoeven, Phys. Rev. B **54**, 10 880 (1996).
[18] J. Erlebacher, M. J. Aziz, E. Chason, M. B. Sinclair, and J. A. Floro, Phys. Rev. Lett. **82**, 2330 (1999).
[19] J. Erlebacher, M. J. Aziz, E. Chason, M. B. Sinclair, and J. R. Floro, J. Vac. Sci. Technol. A **18**, 115 (2000).
[20] S. Habenicht, Phys. Rev. B **63**, 125419 (2001).
[21] I. Koponen, M. Hautala, and O. P. Sievänen, Nucl. Instrum. Methods Phys. Res. B **129**, 349 (1997).
[22] J. Koch, K. Grün, M. Ruff, R. Wernhardt, and A. D. Wieck, Proceedings IECON '99 San Josi (USA) IEEE.
[23] C. Wiemann, M. Versen, and A. D. Wieck, J. Vac. Sci. Technol. B **16**, 2567 (1998).

[24] U. Dötsch and A. D. Wieck, Nucl. Instrum. Methods Phys. Res. B **139**, 12 (1998).
[25] J. Melngailis, J. Vac. Sci. Technol. B **5**, 469 (1987).
[26] J. Orloff, Rev. Sci. Instrum. **64**, 1105 (1993).
[27] P. D. Prewitt and G. L. R. Mair, *Focused Ion Beams from Liquid Metal Sources* (Research Studies, Taunton, 1991).
[28] M. Nastasi, J. W. Mayer, and J. K. Hirvonen, *Ion-Solid Interactions, Fundamentals and Applications* (Cambridge Solid State Science Series, Cambridge, 1996).
[29] T. S. Mayer, E. Chason, and A. J. Howard, J. Appl. Phys. **76**, 1633 (1994).
[30] R. Cuerno, H. A. Makse, S. Tomassone, S. T. Harrington, and H. E. Stanley, Phys. Rev. Lett. **75**, 4464 (1995).
[31] S. Park, B. Kahng, H. Jeong, and A.-L. Barabasi, Phys. Rev. Lett. **83**, 3486 (1999).
[32] S. Rusponi, G. Costantini, C. Boragno, and U. Valbusa, Phys. Rev. Lett. **81**, 4148 (1998).
[33] M. Kardar, G. Parisi, and Y. C. Zhang, Phys. Rev. Lett. **56**, 889 (1986).
[34] See AIP Document No. E-PAPS: E-PRBMDO-65-032211, 527901 for Postscript and PDF versions of this appendix and supporting documentation. E-PAPS document files may be retrieved free of charge from our FTP server (http://www.aip.org/pubservs/paps.html) or from ftp.aip.org in the directory epaps/. For further information, e-mail: paps@aip.org or fax: 516-576-2223.